A global off-line model of size-resolved aerosol microphysics: I. Model development and prediction of aerosol properties

D. V. Spracklen, K. J. Pringle, K. S. Carslaw, M. P. Chipperfield, G. W. Mann

Atmos. Chem. Phys. Discuss., 5, 179–215, 2005
www.atmos-chem-phys.org/acpd/5/179/
SRef-ID: 1680-7375/acpd/2005-5-179
European Geosciences Union

Atmospheric Chemistry and Physics Discussions

A global off-line model of size-resolved aerosol microphysics: I. Model development and prediction of aerosol properties

D. V. Spracklen, K. J. Pringle, K. S. Carslaw, M. P. Chipperfield, and G. W. Mann

The School of Earth and Environment, University of Leeds, UK

Received: 2 November 2004 – Accepted: 20 December 2004 – Published: 14 January 2005

Correspondence to: D. V. Spracklen (dominick@env.leeds.ac.uk)

Abstract

A GLObal Model of Aerosol Processes (GLOMAP) has been developed as an extension to the TOMCAT 3-D Eulerian off-line chemical transport model. GLOMAP simulates the evolution of the global aerosol size distribution using a sectional two-moment scheme and includes the processes of aerosol nucleation, condensation, growth, coagulation, wet and dry deposition and cloud processing. We describe the results of a global simulation of sulfuric acid and sea spray aerosol. The model captures features of the aerosol size distribution that are well established from observations in the marine boundary layer and free troposphere. Modelled condensation nuclei (CN>3 nm) vary between about 250–500 cm^{-3} in remote marine boundary layer regions and between 2000 and 10 000 cm^{-3} (at standard temperature and pressure) in the upper troposphere. Cloud condensation nuclei (CCN) at 0.2% supersaturation vary between about 1000 cm^{-3} in polluted regions and between 10 and 500 cm^{-3} in the remote marine boundary layer. New particle formation through sulfuric acid-water binary nucleation occurs predominantly in the upper troposphere, but the model results show that these particles contribute greatly to aerosol concentrations in the marine boundary layer. It is estimated that sea spray emissions account for only ∼10% of CCN in the tropical marine boundary layer, but between 20 and 75% in the mid-latitude Southern Ocean.

1. Introduction

Particles in the atmosphere contribute to radiative forcing directly by scattering and absorbing radiation, and indirectly by altering the properties of clouds. The latest Intergovernmental Panel on Climate Change report (IPCC, 2001) estimated the direct forcing of anthropogenic aerosols to be $-0.5\,Wm^{-2}$ and the indirect forcing to lie between 0 and $-2\,Wm^{-2}$. These forcings are comparable, but opposite in sign, to the forcing of anthropogenic greenhouse gases.

ACPD

5, 179–215, 2005

The effect of changes in aerosol properties on clouds is a particularly uncertain quantity in climate simulations and also presents the greatest modelling challenge because of the many factors that control the links between aerosol properties and cloud properties. The most fundamental, though by no means only, quantity that needs to be accurately prognosed in a model is the concentration of cloud condensation nuclei (CCN) – the subset of the aerosol, usually the largest, that can form cloud droplets at a particular supersaturation. The CCN number depends on the concentration and composition of particles greater than about 50 nm dry diameter, which is a size range that is influenced by primary particle production and by secondary particles that have grown to this size through condensation and coagulation processes on the timescale of days to weeks. The response of CCN concentrations to changes in the emissions of primary particles and precursor gases is therefore likely to be complex.

In order to make a better estimate of the indirect effect it is important to understand the factors that control the number of CCN at a given supersaturation in a cloud. However, early global aerosol models were not able to simulate the particle size distribution and only predicted the mass of certain particle classes, such as sulfate (e.g., Langner and Rodhe, 1991; Jones et al., 1994, 2001; Chin et al., 1996; Pham et al., 1995; Feichtrer et al., 1997; Koch et al., 1999; Barth et al., 2000; Rasch et al., 2000) or carbonaceous material e.g., (Cooke and Wilson, 1996; Tegen et al., 2000). Early climate simulations relied on empirical relationships between aerosol mass and CCN concentration (e.g., Jones et al., 1994, 2001). Although such schemes are computationally efficient for long climate change simulations and exploit the aerosol information in the model, they do not capture the dependence of cloud droplet concentration on aerosol properties that has been observed globally (Ramanathan et al., 2001). More recently models have been developed that are capable of a size-resolved description of sea spray particles (Gong et al., 1997) and sulfate aerosol (Adams and Seinfeld, 2002). Development of size-resolved models of aerosol concentration brings with it the need to include the microphysical processes such as nucleation, condensation, coagulation and cloud processing that affect the size distribution. Although the global

simulation of a fully size-resolved multicomponent aerosol is currently too numerically demanding for centennial scale climate model simulations, these models are essential tools for understanding what controls the microphysical – and ultimately the radiative and cloud-nucleating – properties of the global aerosol. As we show here, the evolution of the size distribution and the factors that control CCN can be examined on timescales as short as 1 month, which is approximately the lifetime of the global aerosol.

This paper is the first of three papers describing a new GLObal Model of Aerosol Processes (GLOMAP). This first paper describes the model and the global simulations of aerosol properties. The second paper, in preparation, will examine in detail the sensitivity of the predicted aerosol size distribution to uncertainties in the driving microphysical processes. The third paper, in preparation, will present a detailed comparison of the model against aerosol observations. The GLOMAP model described here is currently restricted to sea spray and sulfate aerosol.

Section 2 gives a description of the model. Section 3 describes the simulated global fields of sulfur species. Section 4 describes the simulated global aerosol properties.

2. Model description

2.1. The TOMCAT chemical transport model

GLOMAP is an extension to the 3-D off-line Eulerian chemical transport model, TOMCAT, which is described in e.g. Stockwell and Chipperfield (1999). TOMCAT is forced by meteorological analyses and can be run at a a range of resolutions and with different options for physical and chemical parameterisations. These options include a a comprehensive tropospheric chemistry scheme.

2.1.1. Meteorology

The model domain is global and the resolution used here is 2.8°×2.8° latitude × longitude with 31 hybrid σ-p levels extending from the surface to 10 hPa. The vertical

geometric resolution varies from 60 m within the planetary boundary layer to 1 km at the tropopause. In the experiments performed here large-scale atmospheric transport is specified from European Centre for Medium-Range Weather Forecasts (ECMWF) analyses at 6-hourly intervals. Tracer advection is performed using the Prather advection scheme (Prather, 1986), which conserves second-order moments of the tracer field. The non-local vertical diffusion scheme of Holtslag and Boville (1993) calculates the planetary boundary layer height and eddy diffusion coefficients and is capable of representing convective turbulence. Sub-grid scale moist convection is parametrised using the scheme of Tiedtke (1989). Precipitation occurs due to sub-grid convective processes (also following Tiedtke, 1989) and due to frontal (or large scale) processes according to the scheme of Giannakopoulos et al. (1999).

2.1.2. Gas phase chemistry

The chemical reactions included in the model are listed in Table 1. Concentrations of OH, NO_3, H_2O_2 and HO_2 are specified using 6-hourly monthly mean 3-D concentration fields from a TOMCAT run with detailed tropospheric chemistry and linearly interpolated onto the model timestep. The chemical scheme in Table 1 is considered the minimum necessary to examine the sulfur cycle and sulfate aerosol formation. Time-dependent chemical rate equations are solved using the IMPACT algorithm of the ASAD software package (Carver et al., 1997).

GLOMAP includes SO_2 emissions from anthropogenic and volcanic sources and dimethyl sulfide (DMS) emissions from the ocean. Anthropogenic emissions are taken from the Global Emissions Inventory Activity (GEIA) database (Benkovitz et al., 1996), which are seasonally averaged and based on the year 1985. In the baseline model runs presented here all the emitted sulfur is assumed to be SO_2, but in Spracklen et al. (in preparation, 2005)[1] we also explore the sensitivity of modelled aerosol to

[1]Spracklen, D., Pringle, K., Carslaw, K., Chipperfield, M., and Mann, G.: A global off-line model of size resolved aerosol processes, II. Importance of uncertainties in microphysical pro-

small amounts of primary sulfate aerosol. The emissions inventory classifies emissions as occurring above or below 100 m. The emissions are partitioned linearly onto the appropriate model grid levels according to the thickness of the model levels.

Oceanic DMS emissions are calculated using the monthly mean seawater DMS concentration database of Kettle et al. (1999) and the sea-to-air transfer velocity of Liss and Merlivat (1986). The wind speed at 10 m, which is needed for the calculation of transfer velocity, is calculated from the ECMWF analyses used to force the model assuming a neutral surface layer and a roughness length of 0.001 m for the sea surface.

Volcanic emissions of SO_2 are obtained from Andres and Kasgnoc (1998) and injected at a constant rate between pressure levels of 880 and 350 hPa (Jones et al., 2001). Sporadically erupting volcanoes are not included in the model. All volcanic emissions are assumed to be SO_2.

2.2. The aerosol microphysics module

2.2.1. The aerosol size distribution

The aerosol size distribution is simulated using the moving-centre scheme of Jacobson (1997a), which is often termed a two-moment sectional scheme. In this scheme the average mass per particle in each size section (or bin) as well as the total number concentration in the bin are carried (mass and number being the 2 moments). Within each section, the average particle size varies between the lower and upper bin edges as mass is added to, or removed from, the particles, for example due to condensation and evaporation. If the average particle mass in a bin exceeds its fixed bin edge the total mass and number of particles in this bin is added to the appropriate new bin (not necessarily the adjacent one). The number concentration of the original bin is set to zero and its average mass re-set to the mid-point mass. Such a two-moment scheme explicitly describes the growth of a size distribution in terms of changes in the mass of the particles in a bin. In contrast, in a single-moment number-only scheme growth

cesses, Atmos. Chem. Phys. Discuss., in preparation, 2005.

must be described in terms of the change in the number of fixed-size particles in each bin. Two-moment schemes have the advantage of greatly reducing the numerical diffusion (in radius space) that is a characteristic of single-moment number-only schemes (Jacobson, 1997a; Korhonen et al., 2003), but have the disadvantage in a 3-D model that two pieces of information need to be carried to define the size distribution of a single-component aerosol. A multi-component, two-moment scheme results in a large increase in information needing to be carried. However, whilst the number of extra model tracers required to simulate the mass per particle in the two-moment scheme increases linearly with the number of chemical components in each particle only one number concentration is required for each distribution.

The bin centres are geometrically (mass ratio) spaced and span 0.001 to 25 μm equivalent dry diameter. The number of bins can be set arbitrarily, although the number required to capture the principal features of the natural size distribution is about 20 (Gong et al., 2003), which we use here. Water is not included as an aerosol component. Instead, particles are allowed to re-equilibrate with the ambient relative humidity before calculating size-dependent quantities such as the coagulation kernel. The model conserves aerosol number and aerosol mass.

2.2.2. Microphysical processes

These simulations are restricted to sulfuric acid aerosol (formed through gas-to-particle conversion of gaseous H_2SO_4) and sea spray. As a further simplification, these two aerosol types are assumed to have the same physical properties (density and hygroscopic behaviour) and their chemical properties are not simulated (that is, we do not calculate the chemical composition and cation/anion speciation of the particles). The chemical equilibration of mixed electrolytes is a complex and numerically expensive problem to solve in a global model (Jacobson, 1997b) and the effects, in terms of particle size distribution, are likely to be subtle in most parts of the atmosphere.

The number of solute molecules per particle in each size bin is converted to a particle volume using the Köhler equation appropriate for sulfuric acid-water mixtures and rel-

ative humidities from the meteorological analyses. The assumption that the sea spray particles have the same hygroscopic properties as sulfuric acid will lead to a factor 1.33 difference in the diameter of the particles under humid oceanic conditions where most of the sea spray particles reside (Gong et al., 2003).

New particle formation is treated using the binary H_2SO_4-H_2O nucleation scheme of Kulmala et al. (1998). New particles are assumed to nucleate at a size of 100 molecules of H_2SO_4 per particle. Condensation of H_2SO_4 onto all particles is calculated using the modified Fuchs-Sutugin equation (Fuchs and Sutugin, 1971). The noncontinuum effect that occurs during condensation onto small particles is accounted for using a correction factor which is a function of the Knudsen number. The accommodation coefficient, a_e, is assumed to have a value of unity, although the sensitivity of the aerosol distribution to the magnitude of a_e is explored in Spracklen et al. (in preparation, 2005)[1].

Coagulation of particles is calculated using the mass conserving semi-implicit numerical solution of Jacobson et al. (1994). The coagulation kernels account only for Brownian diffusion, which is the dominant mechanism for submicron particles. Kernels are calculated using the size of the particles after equilibration with water.

Dry deposition of aerosols is based on the schemes of Slinn and Slinn (1981) and Zhang et al. (2001). It includes the deposition processes of gravitational settling, Brownian diffusion, impaction, interception and particle rebound.

In-cloud aqueous phase oxidation of SO_2 to form aqueous H_2SO_4 is calculated in grid boxes that contain low stratiform cloud according to global fields from the International Satellite Cloud Climatology Project D1 database (Rossow and Schiffer, 1999). We assume that particles with a dry diameter larger than 0.05 μm activate. The maximum rate of aqueous oxidation is set by the rate of diffusion of SO_2 onto the activated particle distribution, which is calculated using the Fuchs-Sutugin equation (Fuchs and Sutugin, 1971). Available SO_2 is reacted stoichiometrically with H_2O_2 and the concentrations of both are reduced accordingly. Sulfate is added to the particle distribution and partitioned between different size bins depending on the rates of SO_2 diffusion to each particle size bin. If H_2O_2 concentrations were allowed to return to the prescribed

values at the end of each time step this would cause an overprediction of H_2O_2 oxidation rates. Instead H_2O_2 is replenished using the prescribed concentration of HO_2 (Jones et al., 2001).

The emission of sea spray particles is calculated using the parametrisation of Gong (2003), which produces realistic emissions at particle sizes between 0.07 and 20 μm at 80% humidity (corresponding to approximately 0.035 and 10 μm dry diameter). This parametrisation is an extension of the semi-empirical formulation of Monahan et al. (1986) to below 0.2 μm diameter, where the original parametrisation was found to overestimate emissions of sub-micron sea spray particles. The adjustable parameter (Θ) that controls sub-micron emissions is set at 30.

GLOMAP includes description of both in-cloud and below-cloud aerosol wet deposition (due to both convective and frontal precipitation). The in-cloud (or nucleation) scavenging scheme assumes a removal rate of activated aerosol that is proportional to the amount of condensate converted to rain in each timestep. Below-cloud scavenging (impaction by raindrops) is parameterised following Slinn (1983) with scavenging coefficients taken from Beard and Grover (1974). The raindrop distribution is assumed to follow the Marshall-Palmer distribution (with the sophistication of Sekhon and Srivastava, 1971) and is described with seven geometrically spaced raindrop bins.

2.2.3. Numerical treatment

The differential equations that govern the particle mass and number concentration in each size section are solved using operator splitting. This technique has been widely used in large-scale atmospheric models and has the advantage of being considerably cheaper in CPU usage compared to the fully coupled solution. The accuracy of the operator splitting depends on the length of the timestep used. A flowchart of the microphysical operations in GLOMAP is shown in Fig. 1. The TOMCAT model timestep is split into a number of shorter subtimesteps that account for the time scales on which the different microphysical processes operate. The advection timestep is usually 1800 s. This is split into NCTS timesteps (normally 2) over which the emissions and chem-

istry are solved. This timestep is then further split into NMTS timesteps (normally 2) over which the aerosol microphysics is solved. To accurately represent the competition between nucleation and condensation processes this microphysics timestep is subdivided further into NNTS timesteps (normally 5) where condensation and nucleation are calculated.

The accuracy of operator splitting has been tested by changing the length of the different timesteps and the order of operations. Changing the order of operations or further reducing the timestep length changes total aerosol number concentrations by less than 5%.

2.3. Model experiments

The runs were forced by ECMWF analyses. The model runs shown here are for December 1995 and July 1997. The model was spun up from an aerosol-free atmosphere (on 1 October 1995 and 1 May 1997) for a period of 60 days before model output was used. This length of time is sufficient so that model simulations are independent of the model initialisation fields.

3. Global sulfur species

We now briefly describe the model fields of gaseous sulfur species as an aid to understanding the distribution of aerosol in Sect. 4.

Figure 2 shows simulated surface level DMS concentrations. DMS concentrations are highest over oceanic areas (between 5 and 2000 pptv) due to oceanic DMS emissions, and very low over terrestrial areas (less than 5 pptv). The model does not include any terrestrial emissions of DMS and so will tend to underpredict DMS concentrations over land. However, continental emissions of DMS are small and this should not be significant (Pham et al., 1995). The lifetime of DMS is approximately 1 day so its distribution is strongly governed by its sources, and atmospheric DMS concentrations in the

marine boundary layer (MBL) closely follow the DMS concentrations in seawater. The simulations show the strong seasonal variability in atmospheric DMS concentrations caused by the cycle in biological activity altering sea surface DMS concentrations.

The largest simulated DMS concentrations occur over the tropical oceans and in the 30–60° oceanic belt of the summer hemisphere. This distribution reflects larger DMS emissions in these regions, due to a combination of high ocean surface DMS concentrations and higher wind speeds at the higher latitudes. Maximum values above the equatorial oceans of 300 pptv, and at high SH latitudes during the summer of over 1000 pptv, are calculated. Low DMS sea-surface concentrations in the winter hemisphere cause low DMS emissions and low winter hemisphere atmospheric concentrations. Coastal areas with strong oceanic upwelling (e.g., the Peru upwelling zone) have elevated DMS sea surface concentrations (Kettle et al., 1999) leading to higher atmospheric concentrations. Simulated gas phase DMS concentrations agree with measurements in both the Southern Ocean (e.g. Ayers et al., 1995; Shon et al., 2001; Berresheim et al., 1990; De Bruyn et al., 1998; Nguyen et al., 1990) and tropical regions (e.g. Bandy et al., 1996; Andreae et al., 1985) to within a factor of 2 to 3, which is reasonable considering the similar uncertainty in the gridded emissions (Kettle et al., 1999) and sea-air transfer rates.

Figure 3 shows simulated surface level SO_2 concentrations. Concentrations of SO_2 are high over the United States, Europe and the Far East where there are large emissions from fossil fuel burning. Additional maxima are observed over certain locations in Siberia and in the SH in Africa and South America due to smelting activities. The lifetime of SO_2 is sufficiently long that transport of SO_2 away from these source regions is apparent, particularly from the east coast of the United States and the east coast of Asia. In December the model simulates strong advection of SO_2 from Europe and the United States to regions north of the Arctic circle. The aerosol mass loading is also greatly increased in Arctic regions affected by such transport of anthropogenic SO_2 (see Sect. 4).

The model captures the observed (e.g. Rasch et al., 2000) seasonal cycle of SO_2

over the northern hemisphere (NH), with wintertime concentrations being a factor of two higher than summertime concentrations. This cycle has been explained by higher emissions (over Europe winter emissions in the GEIA inventory are about 30% higher than in summer), lower oxidant concentrations, and a stable boundary layer during winter months (Rasch et al., 2000). In clean marine areas SO_2 concentrations of between 10 and 100 ppt are simulated, with the majority of the SO_2 deriving from DMS oxidation. Concentrations of SO_2 in the SH winter are very low due to low concentrations of DMS. The low concentrations of around 10 ppt in the tropics are due to efficient aqueous phase oxidation and removal in clouds. Simulated SO_2 concentrations agree with measurements both over polluted continental regions (e.g., EMEP, 1989; Shaw and Paur, 1983; Heintzenberg and Larssen, 1983; Barrie and Bottenheim, 1990) and remote oceanic regions (e.g., Ayers et al., 1997; De Bruyn et al., 1998; Bandy et al., 1996) within a factor of 2 to 3.

4. Global aerosol properties

4.1. Global CN and CCN distributions

Figures 4 and 5 show surface and Figs. 6 and 7 zonal mean simulated monthly mean number concentrations of condensation nuclei (CN) and cloud condensation nuclei (CCN). To allow easy comparison with observations CN are reported as the concentration of particles >3 nm diameter, which corresponds to the detection limit of current instruments (Stolzenburg and McMurry, 1991). CCN are reported at 0.2% supersaturation, which is typical of marine stratocumulus clouds, and corresponds to the activation of particles having a dry diameter of about 70 nm. All concentrations have been converted to conditions of standard temperature and pressure (STP, 273 K and 1 atm).

Smallest CN number concentrations are found in remote marine areas and largest concentrations are found near anthropogenically polluted regions. Simulated remote MBL CN concentrations are typically 250–500 cm^{-3}, which compares well with obser-

vations (Clarke et al., 1987; Fitzgerald, 1991; Andreae et al., 1994, 1995; Pandis et al., 1995; Covert et al., 1996; Raes et al., 2000). Over the United States, Europe and East and Central Asia surface CN number concentrations of around 1000–5000 cm^{-3} are simulated. This is somewhat lower than most observations under polluted continental conditions of 5×10^3 and 1×10^5 cm^{-3} (Raes et al., 2000; Pandis et al., 1995). A possible reason for this underprediction of CN concentrations over continental regions is discussed in Spracklen et al. (in preparation, 2005)[1].

Simulated CN concentrations increase with altitude (Fig. 6), with maximum concentrations simulated in the upper troposphere (UT), as has been observed in recent field campaigns (e.g., Clarke et al., 1999) and simulated in models (Adams and Seinfeld, 2002). Simulated UT concentrations in the tropics peak at higher concentrations and at higher altitudes than at mid latitudes.

Simulated CCN concentrations decrease with increasing altitude and concentrations are generally highest in polluted NH regions, with an obvious correlation between CN, CCN and sources of anthropogenic SO_2. Interestingly, CN concentrations are higher in winter than summer while CCN concentrations show the opposite (though less pronounced) seasonal variation. In winter, lower temperatures mean that nucleation can occur over a greater depth of the free troposphere (FT), which leads to higher surface CN concentrations. In summer, higher OH radical concentrations lead to greater production of gas phase sulfuric acid, which causes faster rates of condensational growth (while having little effect on the insignificant binary homogeneous nucleation rate). The lower number of available particles are able to grow faster, leading to higher CCN concentrations. Also apparent in Fig. 6 is the vertical extension of the CCN-rich air into the summer FT, which is caused by more efficient vertical mixing of boundary layer air. CCN concentrations are also clearly depleted along the Inter-Tropical Convergence Zone (ITCZ) due to effective cloud scavenging processes.

Figure 8 shows daily average altitude profiles of CN number and volume concentration over the remote South Pacific Ocean. Simulated CN concentrations increase by about an order of magnitude between the surface and 10 km altitude, as has been

observed in a variety of field campaigns (e.g. Clarke and Kapustin, 2002). Maximum CN concentrations at this location are simulated at around 9 km altitude. Simulated dry volume concentrations are greatest at the surface (1–15 μm^3 cm^{-3}) and decrease with increasing altitude (to about 0.02–0.05 μm^3 cm^{-3} at 10 km), as has been observed (Clarke and Kapustin, 2002). Figure 8 also gives an indication of the instantaneous spatial variability in aerosol number and volume in a limited region. Notice, for example, the greater than 2 orders of magnitude variability in aerosol volume between 1 and 3 km altitude that arises due to cloud scavenging processes.

4.2. Contribution of sea spray to CCN

It is important to quantify the relative contribution of sea spray particles and other aerosols to MBL CCN for several reasons. Firstly, oceanic regions have low natural aerosol concentrations and are therefore susceptible to modification due to inputs from anthropogenic emissions. Secondly, the sea spray source function is particularly uncertain for particles with sizes less than 1 μm, and it is particles of this size that contribute most to the CCN number. Thirdly, the climate response to changes in emissions of DMS depends on the changes in CCN resulting from new sulfate particles in the MBL.

The relative contribution of sea spray and sulfate particles to MBL CCN is uncertain and dependent on locations and atmospheric conditions. Blanchard and Cipriano (1987) measured background MBL sea spray particle concentrations of between 15 and 20 cm^{-3}. O'Dowd et al. (1999) observed that 10% of the accumulation mode aerosol was derived from sea spray particles in the Pacific Ocean MBL (600 km off the coast of California with wind speeds of less than 10 ms^{-1}) and that about 30% of total aerosol concentration was sea salt in the North Atlantic MBL (with wind speed up to 17 ms^{-1}). Yoon and Brimblecombe (2002) used a box model to predict that more than 70% of MBL CCN were derived from sea salt where wind speeds were moderate to high, especially in winter seasons in middle to high latitude regions.

Figure 9 shows the model calculation of the contribution of sea spray to total CCN.

This was calculated by comparing a baseline model run with sulfate and sea spray sources to a run where only sea spray emissions were included. In our model simulations most of the sulfate aerosol formation and growth to CCN sizes occurs in low temperature regions lying well above the MBL, so our estimate of relative contributions to CCN based on two separate simulations is likely to be reasonable. More accurate estimates will be possible in a multicomponent version of GLOMAP currently under development.

In the tropical oceanic MBL the model predicts that sea spray contributes less than 10% to total CCN. The remaining 90% are derived mostly from sulfate particles that formed in the free and upper troposphere. The importance of the UT as a source of tropical MBL aerosol is apparent in a run in which aerosol nucleation was switched off below 3 km, which showed little change in MBL sulfate aerosol (not shown here). In the 30–60° oceanic belt sea spray generally contributes between 20 and 75% of total MBL CCN. In the continental boundary layer sea spray contributes less than 1% to total CCN.

4.3. Particle size distributions

The global aerosol distribution was simulated using 20 aerosol size bins. For simplicity, the results can be displayed as four typical size classes based on dry diameter (D_p): nucleation (D_p<7 nm), Aitken (7 nm<D_p<65 nm), accumulation (65 nm<D_p<700 nm) and coarse particles (D_p>700 nm). Figures 10 and 11 show surface level and zonal mean aerosol concentrations divided into these four size ranges for December and July. These are typically accepted ranges that are convenient for dividing the aerosol distribution. However, it does not imply the presence of genuinely distinct modes in the modelled size distribution.

Coarse mode aerosol concentrations are much greater over oceanic areas because these particles are derived from emission of sea spray. Large particles are subject to fast deposition rates and and are not advected far from their source regions, resulting in strong concentration gradients at land-ocean boundaries. Model emission rates

of sea spray particles depend only on the surface wind speeds, resulting in largest MBL concentrations where wind speeds are fastest: generally in the 30–50° S oceanic belt. Low concentrations are simulated near the equator due to the relatively low wind speeds there and the efficient removal of particles in tropical rain clouds.

Both coarse mode and accumulation mode concentrations are strongly depleted along the ITCZ. This is caused by cloud scavenging and convective precipitation effectively removing these larger particles. In contrast Aitken mode particles are not effectively removed by these processes as they do not serve as cloud condensation nuclei nor are they efficiently impaction scavenged by rain (Andronache, 2003), so no depletion is obvious along the ITCZ.

As with seasonal variation of CN and CCN, in the NH winter Aitken mode concentrations are higher than in the NH summer whereas accumulation mode concentrations are higher in NH summer than NH winter. In the SH winter, concentrations of both Aitken and accumulation mode aerosol are reduced due to the lack of DMS emissions.

The model simulates low concentrations of nucleation mode particles at the surface and their distribution is much more patchy than other size classes. The MBL tends to have temperatures that are too high for H_2SO_4-H_2O binary nucleation to occur. Additionally, the large pre-existing aerosol surface area near the surface means that most of the available H_2SO_4 rapidly condenses onto the existing aerosol rather than forming new particles. In some marine areas concentrations of nucleation mode particles up to 250 cm^{-3} are simulated. These tend to occur in regions of low FT temperatures. Rapid vertical mixing can transport nucleation mode particles produced in the FT to the surface before they grow through coagulation and condensation to larger particles. However, there is a clear absence of nucleation mode aerosol where sulfur sources are very limited (see Figs. 2 and 3) even if FT temperatures are very low. This can be seen over the Antarctic continent during the SH winter where no nucleation mode aerosol is simulated. Examination of daily fields of accumulation mode aerosol in remote marine areas reveals an anti-correlation between accumulation mode number and nucleation mode number (not shown here). This will be due to low accumulation mode number

resulting in low pre-existing particle surface area which allows gas phase H_2SO_4 concentrations to build up.

Nucleation and Aitken mode particle concentrations reach a maximum in the UT, with decreasing concentrations towards the surface. Downward transport of nucleation particles from the UT occurs simultaneously with their growth to Aitken mode particles, through coagulation and condensation. Accumulation mode and coarse mode particles have maximum concentrations at the surface. Coarse mode particles have a strong concentration gradient with altitude, with concentrations 10^3–10^4 times lower at 400 hPa than at the surface. This is due to very efficient removal processes by dry and wet deposition. As the model does not simulate gravitational settling of large particles from the upper to lower levels it is possible that the model overestimates the transport of large particles to higher altitudes. Accumulation mode particles are less efficiently removed and are transported to higher altitudes.

Figure 12 shows number and volume distributions as a function of dry particle diameter for December and July. For the North Atlantic MBL and FT, observed size distributions from Raes et al. (2000) are included for comparison. These observations are chosen as they are a climatology rather than measurements over a specific time period.

In the MBL the model captures the characteristic submicron bimodal number-size distribution (the smaller mode at about 20–80 nm diameter and the the larger mode between 100–500 nm diameter) and an additional mode in the supermicron range (Fitzgerald, 1991).

In the FT (at 2.3 km altitude) the model shows a typical FT unimodal distribution of particle concentration. However, comparison of model simulations with observations from Raes et al. (2000) over the North Atlantic shows that the model tends to emphasise a large (sea spray) mode at >1 μm which is not distinct in the observations.

The modelled North Atlantic size distribution is strongly perturbed by anthropogenic sulfur emissions, which, in both summer and winter, dominate the natural emissions. Aitken and accumulation mode particle concentrations greatly exceed those in the

Southern Ocean where natural emissions dominate. The Southern Ocean nucleation and Aitken mode particles also show a lack of growth compared with those in the North Atlantic. Particle growth is even more limited in the Antarctic regions due to the very low sulfuric acid gas concentrations there.

5. Conclusions

A new global off-line aerosol microphysics chemical transport model incorporating a sectional treatment of the aerosol size distribution has been used to simulate the atmospheric distributions of sulfur gases and sulfate and sea spray aerosol. The global tropospheric aerosol was created in the model by spinning up from an initially aerosol-free atmosphere over a period of 60 days. This period is long enough for the aerosol size distribution in all parts of the atmosphere to become insensitive to the length of spin-up.

In the current configuration of the model we have simulated only sea spray and sulfate aerosol, with the latter formed through binary homogeneous nucleation. The model simulates realistic MBL CN concentrations of 250–500 cm^{-3} over remote regions and 1000–5000 cm^{-3} immediately downwind of continental pollution sources. While CN concentrations in remote marine regions are broadly in agreement with observations, those in polluted regions are somewhat lower than suggested by observations. Possible explanations for this disparity are examined in Spracklen et al. (in preparation, 2005)[1]. The UT and FT are the dominant source regions for new sulfuric acid particles due to the low temperatures there, which accelerate the rate of binary homogeneous nucleation (Kulmala et al., 1998). These new particles grow through coagulation and condensation as they are transported downwards through the FT and provide a source of particles up to 100 nm dry diameter above the MBL. The FT particle size distribution is monomodal, while in the MBL the model simulates the typical trimodal distribution with Aitken, accumulation and coarse modes occurring at approximately the correct sizes and number concentrations. The model supports the hypothesis that MBL parti-

cle number is sustained by entraining particles which have nucleated in the FT.

References

Adams, P. and Seinfeld, J.: Predicting global aerosol size distributions in general circulation models, J. Geophys. Res.-A, 107, 4370–4393, 2002. 181, 191

Andreae, M., Ferek, R., Bermond, F., Byrd, K., Engstrom, T., Hardin, S., Houmere, P., LeMarrec, F., Raemdonck, H., and Chatfield, R.: Dimethyl sulfide in the marine atmosphere, J. Geophys. Res.-A, 90, 12 891–12 900, 1985. 189

Andreae, T., Andreae, M., and Schebeske, G.: Biogenic sulfur emissions and aerosol over the tropical South Atlantic, 1. Dimethylsulfide in seawater and in the atmospheric boundary layer, J. Geophys. Res.-A, 99, 22 819–22 829, 1994. 191

Andreae, M., Elbert, W., and de Mora, S.: Biogenic sulfur emissions and aerosols over the tropical South Atlantic, 3. Atmospheric dimethylsulfide, aerosols and cloud condensation nuclei, J. Geophys. Res.-A, 100, 11 335–11 356, 1995. 191

Andres, R. and Kasgnoc, A.: A time-averaged inventory of subaerial volcanic sulfur emissions, J. Geophys. Res.-A, 103, 25 251–25 261, 1998. 184

Andronache, C.: Estimated variability of below-cloud aerosol removal by rainfall for observed aerosol size distributions, Atmos. Chem. Phys., 3, 131–143, 2003, SRef-ID: 1680-7324/acp/2003-3-131. 194

Atkinson, R., Baulch, D., Cox, A., Hampson Jr., R., Derr, J., and Troe, J.: Evaluated kinetics and photochemical data for atmospheric chemistry: Supplement III, J. Phys. Chem. Ref. Data, 88, 881–1097, 1989. 203

Ayers, G., Bentley, S., Ivey, J., and Forgan, B.: Dimethylsulfide in marine air at Cape Grim, 41° S, J. Geophys. Res.-A, 100, 21 013–21 021, 1995. 189

Ayers, G., Cainey, J., Gillett, R., Saltzman, E., and Hooper, M.: Sulfur dioxide and dimethyl sulfide in marine air at Cape Grim, Tasmania, Tellus, 49B, 292–299, 1997. 190

Bandy, A., Thornton, D., Blomquist, B., Chen, S., Wade, T., Ianni, J., Mitchell, G., and Nadler, W.: Chemistry of dimethyl sulfide in the equatorial Pacific atmosphere, Geophys. Res. Lett., 23, 741–744, 1996. 189, 190

Barrie, L. and Bottenheim, J.: Pollution in the arctic atmosphere, chap. Sulphur and Nitrogen Pollution in the Arctic Atmosphere, 151–181, Elsevier, 1990. 190

Barth, M., Rasch, P., Kiehl, J., Benkovitz, C., and Schwartz, S.: Sulfur chemistry in the National Center for Atmospheric Research Community Climate Model: Description, evaluation, features, and sensitivity to aqueous chemistry, J. Geophys. Res.-A, 105, 1387–1415, 2000. 181

Beard, K. and Grover, S.: Numerical collision efficiencies for small raindrops colliding with micron size particles, J. Atmos. Sci., 31, 543–550, 1974. 187

Benkovitz, C., Scholtz, M., Pacyna, J., Tarrasón, L., Dignon, J., Voldner, E., Spiro, P., Logan, J., and Graedel, T.: Global gridded inventories of anthropogenic emissions of sulfur and nitrogen, J. Geophys. Res.-A, 101, 29 239–29 253, 1996. 183

Berresheim, H., Andreae, M., Ayers, G., Gillett, R., Merrill, J., Davis, V., and Chameides, W.: Airborne Measurements of Dimethylsulfide, Sulfur Dioxide, and Aerosol Ions over the Southern Ocean South of Australia, J. Atmos. Chem., 10, 341–370, 1990. 189

Blanchard, D. and Cipriano, R.: Biological regulation of climate, Nature, 330, 526, 1987. 192

Carver, G., Brown, P., and Wild, O.: The ASAD atmsopheric chemistry integration package and chemical reaction database, Computer Physics Communications, 105, 197–215, 1997. 183

Chin, M., Jacob, D., Gardner, G., Foreman-Fowler, M., and Spiro, P.: A Global three-dimensional model of tropospheric sulfate, J. Geophys. Res.-A, 101, 18 667–18 690, 1996. 181

Clarke, A. and Kapustin, V.: A Pacific Aerosol Survey, Part I: A Decade of Data on Particle Production, Transport, Evolution, and Mixing in the Troposphere, J. Atmos. Sci., 59, 363–382, 2002. 192

Clarke, A., Ahlquist, N., and Covert, D.: The Pacific marine aerosol: Evidence for natural acid sulfates, J. Geophys. Res.-A, 92, 4719–4190, 1987. 191

Clarke, A., Eisele, F., Kasputin, V., Moore, K., Tanner, D., Mauldin, L., Litchy, M., Lienert, B., Carroll, M., and Albercook, G.: Nucleation in the equatorial free troposphere: Favorable environments during PEM-Tropics, J. Geophys. Res.-A, 104, 5735–5744, 1999. 191

Cooke, W. and Wilson, J.: A global black carbon aerosol model, J. Geophys. Res.-A, 101, 19 395–19 409, 1996. 181

Covert, D., Kapustin, V., Bates, T., and Quinn, P.: Physical properties of marine boundary layer aerosol particles of the mid-Pacific in relation to sources and meteorological transport, J. Geophys. Res.-A, 101, 6919–6930, 1996. 191

De Bruyn, W., Bates, T., Cainey, J., and Saltzman, E.: Shipboard measurements of dimethyl sulfide and SO_2 southwest of Tasmania during the First Aerosol Characterization Experiment

(ACE 1), J. Geophys. Res.-A, 103, 16 703–16 711, 1998. 189, 190
DeMore, W., Sander, S., Golden, D., Hampson, R., Howard, C., Ravishankara, A., Kolb, C., and Molina, M.: Chemical kinetics and photochemical data for use in stratospheric modeling, Tech. rep., JPL Publ., 1992. 203
EMEP: Airborne transboundary transport of sulfur and nitrogen species over Europe – model descriptions and calculations, Tech. Rep. 80, EMEP, 1989. 190
Feichtrer, J., Lohmann, U., and Schult, I.: The atmospheric sulfur cycle in ECHAM-4 and its impact on short wave radiation, Climate Dynamics, 13, 235–246, 1997. 181
Fitzgerald, J.: Marine aerosols: A review, Atmos. Envir., 25, 533–545, 1991. 191, 195
Fuchs, N. and Sutugin, A.: Topics in Current Aerosol Research, chap. Highly dispersed aerosols, 1–60, Pergemon, 1971. 186
Giannakopoulos, G., Chipperfield, M., Law, K., and Pyle, J.: Validation and intercomparison of wet and dry deposition schemes using ^{210}Pb in a global three-dimensional off-line chemical transport model, J. Geophys. Res.-A, 104, 23 761–23 784, 1999. 183
Gong, S.: A parameterization of sea-salt aerosol source function for sub- and super-micron particles, Global Biogeochem. Cycles, 17, 1097–1103, 2003. 187
Gong, S., Barrie, L., and Blanchet, J.-P.: Modeling sea-salt aerosols in the atmosphere, 1. Model Development, J. Geophys. Res.-A, 102, 3805–3818, 1997. 181
Gong, S., Barrie, L., Blanchet, J.-P., von Salzen, K., Lohmann, U., Lesins, G., Spacek, L., Zhang, L., Girard, E., Lin, H., Leaitch, R., Leighton, H., Chylek, P., and Huang, P.: Canadian Aerosol Module: A size-segregated simulation of atmospheric aerosol processes for climate and air quality models 1. Module development, J. Geophys. Res.-A, 108, 4007–4023, 2003. 185, 186
Heintzenberg, J. and Larssen, S.: SO_2 and SO_4 in the arctic: interpretation of observations at three Norwegian arctic-subarctic stations, Tellus, 35B, 255–265, 1983. 190
Holtslag, A. and Boville, B.: Local versus nonlocal boundary layer diffusion in a globl climate model, J. Clim., 6, 1825–1842, 1993. 183
IPCC: Radiative Forcing of Climate Change, Tech. rep., Intergovernmental Panel on Climate Change, 2001. 180
Jacobson, M.: Development and Application of a new air pollution modeling system, Part II: Aerosol module structure and design, Atmos. Envir., 31A, 131–144, 1997a. 184, 185
Jacobson, M.: Numerical techniques to solve condensational and dissolutional growth equations when growth is coupled to reversible aqueous reactions, Aerosol Sci. Technol., 491–

498, 1997b. 185
Jacobson, M., Turco, R., Jensen, E., and Toon, O.: Modeling coagulation among particles of different composition and size, Atmos. Envir., 28A, 1327–1338, 1994. 186
Jones, A., Roberts, D., and Slingo, A.: A climate model study of indirect radiative forcing by anthropogenic sulfate aerosols, Nature, 370, 450–453, 1994. 181
Jones, A., Roberts, D., Woodage, M., and Johnson, C.: Indirect sulphate aerosol forcing in a climate model with an interactive sulphur cycle, J. Geophys. Res.-A, 106, 20 293–20 310, 2001. 181, 184, 187
Kettle, A., Andreae, M., Armouroux, D., Andreae, T., Bates, T., Berresheim, H., Bingemer, H., Boniforti, R., Curran, M., DiTullio, G., Helas, G., Jones, G., Keller, M., Kiene, R., Leck, C., Levasseur, M., Malin, G., Maspero, M., Matrai, P., McTaggart, A., Mihalopoulos, N., Nguyen, B., Novo, A., Putaud, J., Rapsomanikis, S., Roberts, G., Schebeske, G., Sharma, S., Simö, R., Staubes, R., Turner, S., and Uher, G.: A global database of sea surface dimethylsulfide (DMS) measurements and a procedure to predict sea surface DMS as a function of latitude, longitude and month, Global Biogeochem. Cycles, 13, 399–444, 1999. 184, 189
Koch, D., Jacob, D., Tegen, I., Rind, D., and Chin, M.: Tropospheric sulfur simulation and sulfate direct radiative forcing in the Goddard Institute for Space Studies general circulation model, J. Geophys. Res.-A, 104, 23 799–23 822, 1999. 181
Korhonen, H., Lehtinen, K., Pirjola, L., Napari, I., and Vehkamäki, H.: Simulation of atmospehric nucleation mode: A comparison of nucleation models and size distribution representations, J. Geophys. Res.-A, 108, 4471–4479, 2003. 185
Kulmala, M., Laaksonen, A., and Pirjola, L.: Parameterizations for sulfuric acid/water nucleation rates, J. Geophys. Res.-A, 103, 8301–8307, 1998. 186, 196
Langner, J. and Rodhe, H.: A Global Three-Dimensional Model of the Troposheric Sulfur Cycle, J. Atmos. Chem., 13, 225–263, 1991. 181
Liss, P. and Merlivat, L.: The Role of Air-Sea Exchange in Geochemical Cycling, chap. Air-sea gas exchange rates: Introduction and synthesis, 113–127, D. Reidel, Norwell, Mass., 1986. 184
Monahan, E., Spiel, D., and Davidson, K.: Oceanic Whitecaps, chap. A model of marine aerosol generation via whitecaps and wave disruption, 167–174, D. Reidel, Norwell, Mass., 1986. 187
Nguyen, B., Mihalopoulos, N., and Belviso, S.: Seasonal variation of atmospheric dimethylsulfide at Amsterdam Island in the Southern Indain Ocean, J. Atmos. Chem., 11, 123–141,

1990. 189
O'Dowd, C., Lowe, J., Smith, M., and Kaye, A.: The relative importance of non-sea-salt sulphate and sea-salt aerosol to the marine cloud condensation nuclei population: An improved multi-component aerosol-cloud droplet parametrization, Q. J. R. Meteorol. Soc., 125, 1295–1313, 1999. 192
Pandis, S., Wexler, A., and Seinfeld, J.: Dynamics of Tropospheric Aerosols, J. Phys. Chem., 99, 9646–9659, 1995. 191
Pham, M., Müller, J., Brasseur, G., Granier, C., and Mégie, G.: A three-dimensional study of tropospheric sulfur cycle, J. Geophys. Res.-A, 100, 26 061–26 092, 1995. 181, 188, 203
Prather, M.: Numerical Advection by Conservation of Second-Order Moments, J. Geophys. Res.-A, 91, 6671–6681, 1986. 183
Raes, F., Van Dingenen, R., Vignati, E., Wilson, J., Putaud, J.-P., Seinfeld, J., and Adams, P.: Formation and cycling of aerosols in the global troposphere, Atmos. Envir., 34, 4215–4240, 2000. 191, 195, 215
Ramanathan, V., Crutzen, P., Kiehl, J., and Rosenfeld, D.: Atmosphere – Aerosols, climate, and the hydrological cycle, Science, 294, 2119–2124, 2001. 181
Rasch, P., Barth, M., Kiehl, J., Schwartz, S., and Benkovitz, C.: A description of the global sulfur cycle and its controlling processes in the National Center for Atmospheric Research Community Climate Model, Version 3, J. Geophys. Res.-A, 105, 1367–1385, 2000. 181, 189, 190
Rossow, W. and Schiffer, R.: Advances in Understanding Clouds From ISCCP, Bulletin of the American Meteorological Society, 80, 2261–2287, 1999. 186
Sekhon, R. and Srivastava, R.: Doppler observations of drop size distributions in a thunderstorm, J. Atmos. Sci., 28, 983–994, 1971. 187
Shaw, R. and Paur, R.: Measurements of sulfur in gases and particles during sixteen months in the Ohio River Valley, Atmos. Envir., 17, 1431–1438, 1983. 190
Shon, Z.-H., Davis, D., Chen, G., Grodzinsky, G., Bandy, A., Thornton, D., Sandholm, S., Bradshaw, J., Stickel, R., Chameides, W., Kok, G., Russell, L., Mauldin, L., Tanner, D., and Eisele, F.: Evaluation of the DMS flux and its conversion to SO_2 over the southern ocean, Atmos. Envir., 35, 159–172, 2001. 189
Slinn, W.: Atmospheric Sciences and Power Production, chap. Precipitation Scavenging, US Department of Energy, 1983. 187
Slinn, S. and Slinn, W.: Atmospheric Pollutants in natural waters, chap. Modeling of atmo-

spheric particulate deposition to natural water, 23–53, Ann. Arbour. Sci., 1981. 186
Stockwell, D. and Chipperfield, M.: A tropospheric chemical-transport model: Development and validation of the model transport schemes, Q. J. R. Meteorol. Soc., 125, 1747–1783, 1999. 182
Stolzenburg, M. and McMurry, P.: An ultrafine aerosol condensation nucleus counter, Aerosol Sci. Tech., 14, 48–65, 1991. 190
Tegen, I., Koch, D., Lacis, A., and Sato, M.: Trends in tropospheric aerosol loads and corresponding impact on direct radiative forcing between 1959 and 1990: A model study, J. Geophys. Res.-A, 105, 26 971–26 989, 2000. 181
Tiedtke, M.: A comprehensive mass flux scheme for cumulus parameterization in large scale models, Mon. Wea. Review, 117, 1779–1800, 1989. 183
Yoon, Y. and Brimblecombe, P.: Modelling the contribution of sea salt and dimethyl sulfide derived aerosol to marine CCN, Atmos. Chem. Phys., 2, 17–30, 2002, SRef-ID: 1680-7324/acp/2002-2-17. 192
Zhang, L., Gong, S., Padro, J., and Barrie, L.: A size-segregated particle dry deposition scheme for an atmospheric aerosol module, Atmos. Envir., 35, 549–560, 2001. 186

Table 1. Sulfur gas phase chemical reactions included in GLOMAP.

Reactions	Reference
$DMS + OH \rightarrow SO_2$	Atkinson et al. (1989)
$DMS + OH \rightarrow 0.6SO_2 + 0.4DMSO$	Pham et al. (1995)
$DMSO + OH \rightarrow 0.6SO_2 + 0.4MSA$	Pham et al. (1995)
$DMS + NO_3 \rightarrow SO_2$	Atkinson et al. (1989)
$H_2S + OH \rightarrow SO_2$	DeMore et al. (1992)
$CS_2 + OH \rightarrow SO_2 + COS$	Pham et al. (1995)
$COS + OH \rightarrow SO_2$	Pham et al. (1995)
$SO_2 + OH + M \rightarrow H_2SO_4$	Pham et al. (1995)

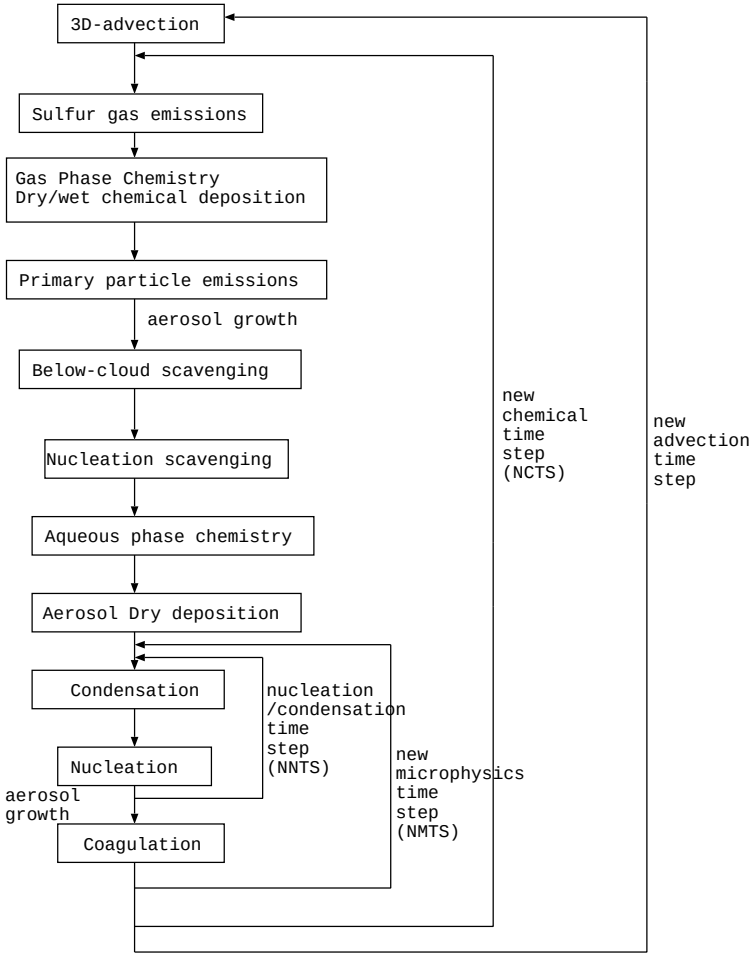

Fig. 1. The flowchart of processes in GLOMAP.

ACPD
5, 179–215, 2005

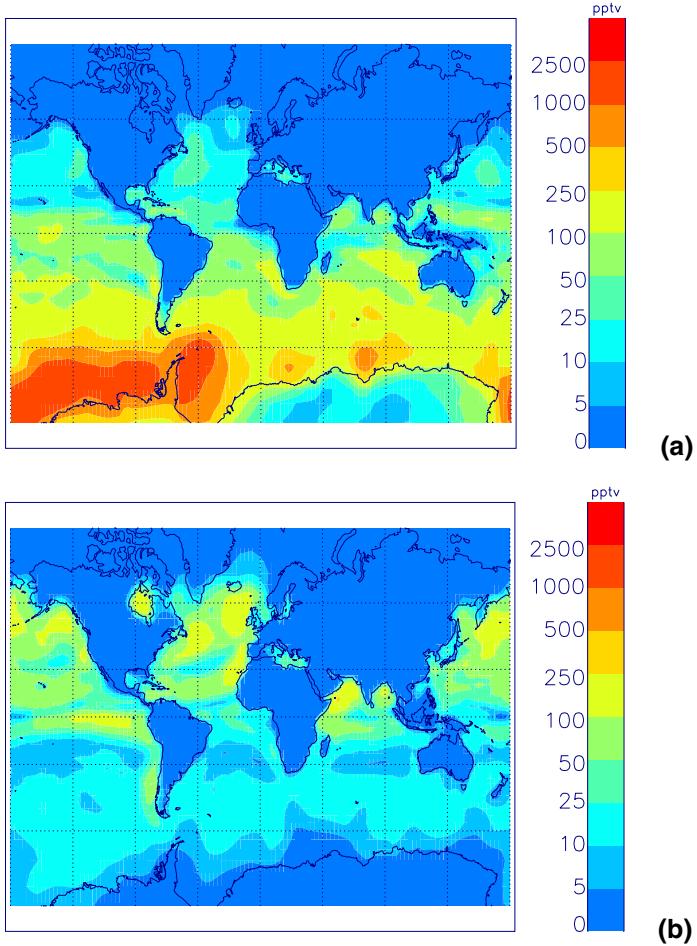

Fig. 2. Simulated monthly mean surface DMS concentrations (in pptv) during **(a)** December 1995 and **(b)** July 1997.

ACPD
5, 179–215, 2005

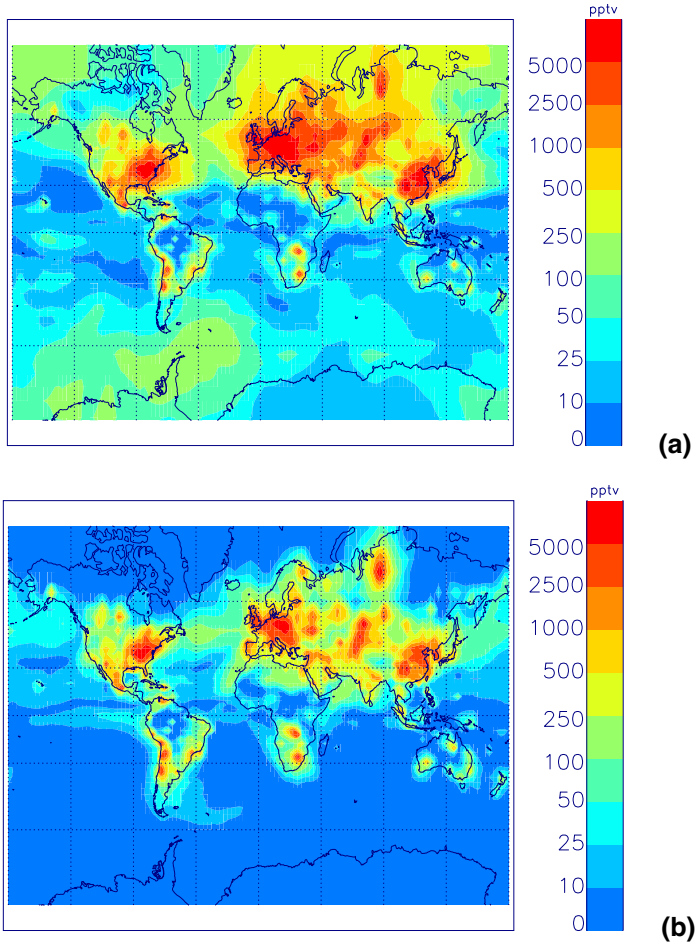

Fig. 3. As for Fig. 2 but for SO_2.

ACPD
5, 179–215, 2005

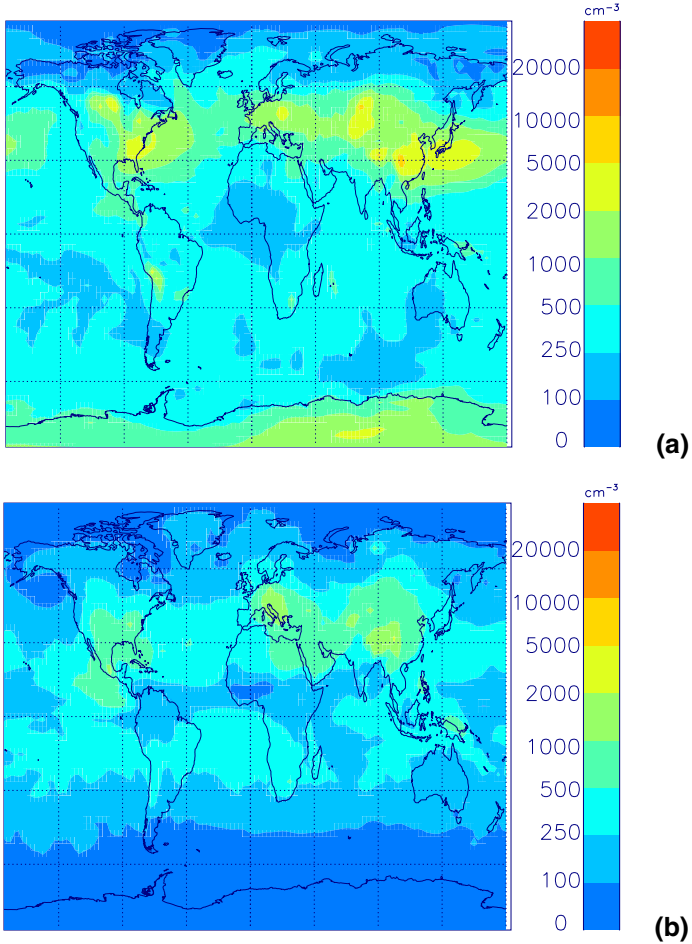

Fig. 4. Simulated monthly mean surface level CN concentrations (cm^{-3}) at standard temperature and pressure for **(a)** December 1995 and **(b)** July 1997.

ACPD
5, 179–215, 2005

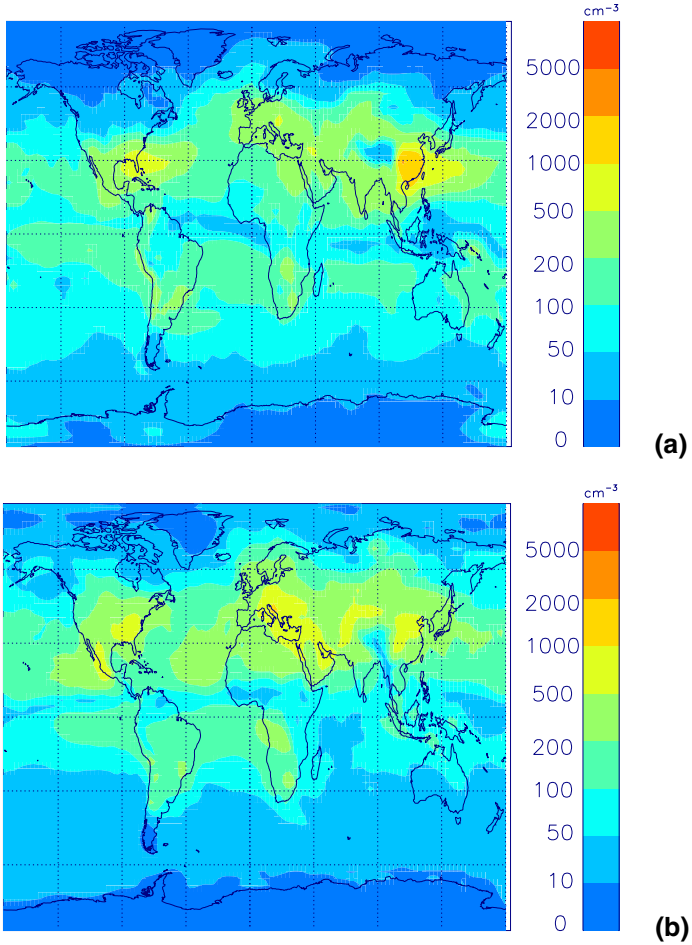

Fig. 5. As for Fig. 4 but for CCN (at 0.2% supersaturation).

ACPD
5, 179–215, 2005

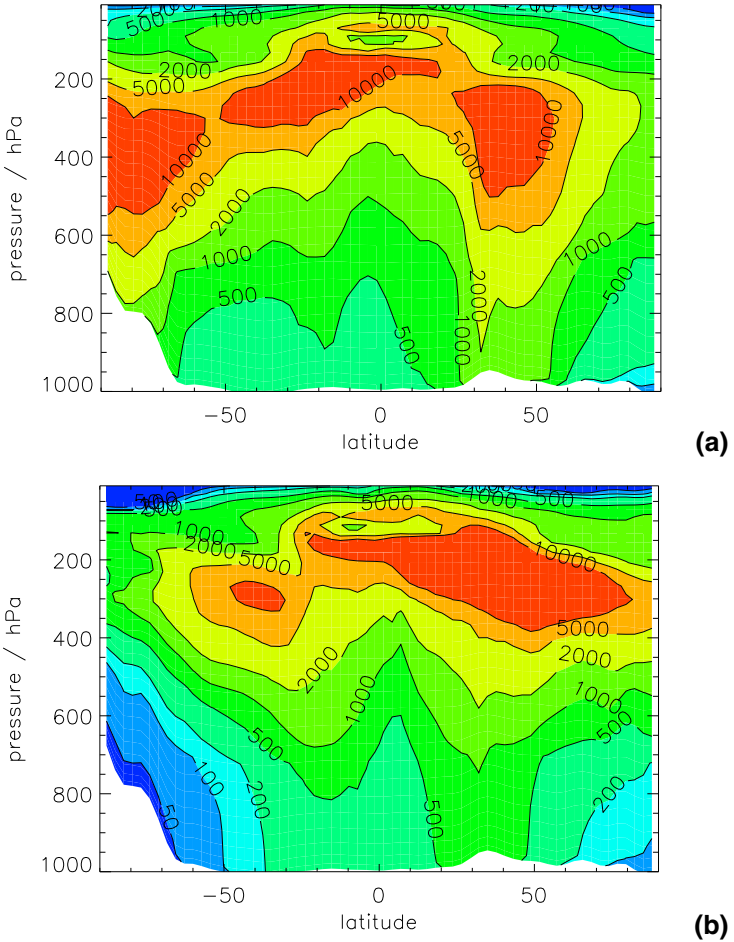

Fig. 6. Simulated zonal monthly mean CN concentrations (cm^{-3}) at standard temperature and pressure for **(a)** December 1995 and **(b)** July 1997.

ACPD
5, 179–215, 2005

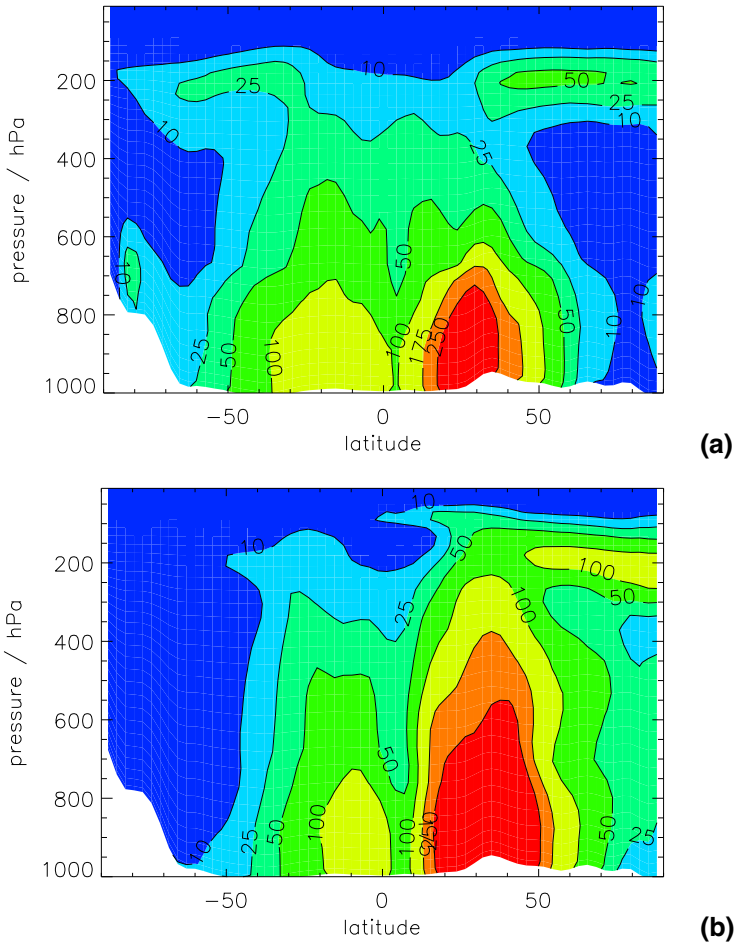

Fig. 7. As for Fig. 6 but for CCN (at 0.2% supersaturation).

ACPD
5, 179–215, 2005

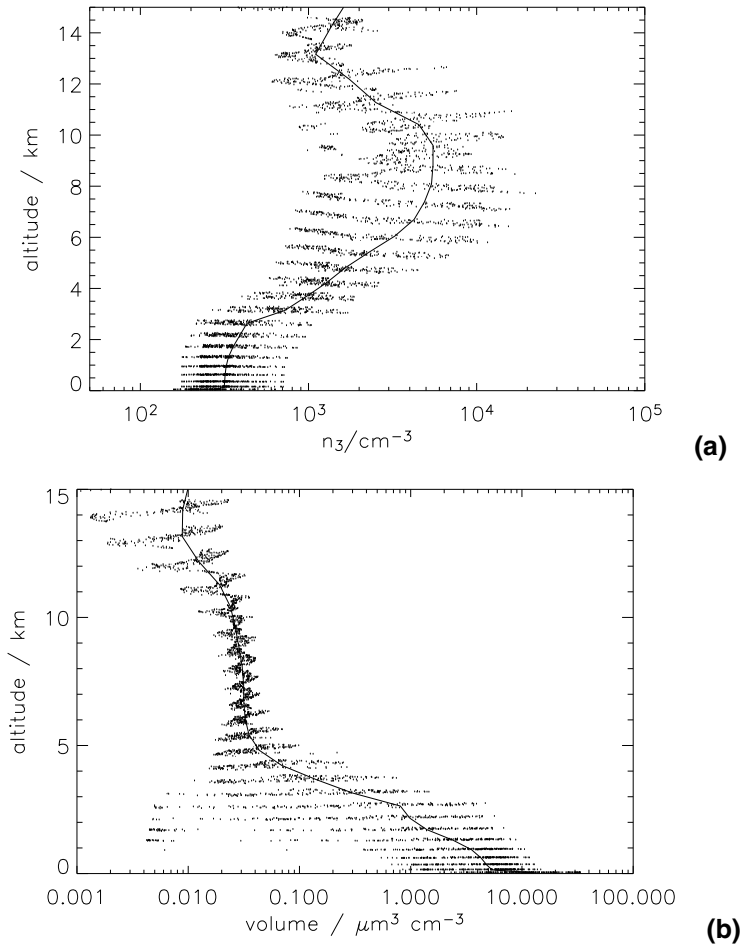

Fig. 8. Daily averaged vertical profiles over the South Pacific (50°–60° S, 210°–270° E) of **(a)** CN number concentrations (cm^{-3}) and **(b)** Volume (μm^3 cm^{-3}) at standard temperature and pressure on 1 December 1995. The solid line shows the spatial mean and the dots show individual 24-h average grid point values.

ACPD
5, 179–215, 2005

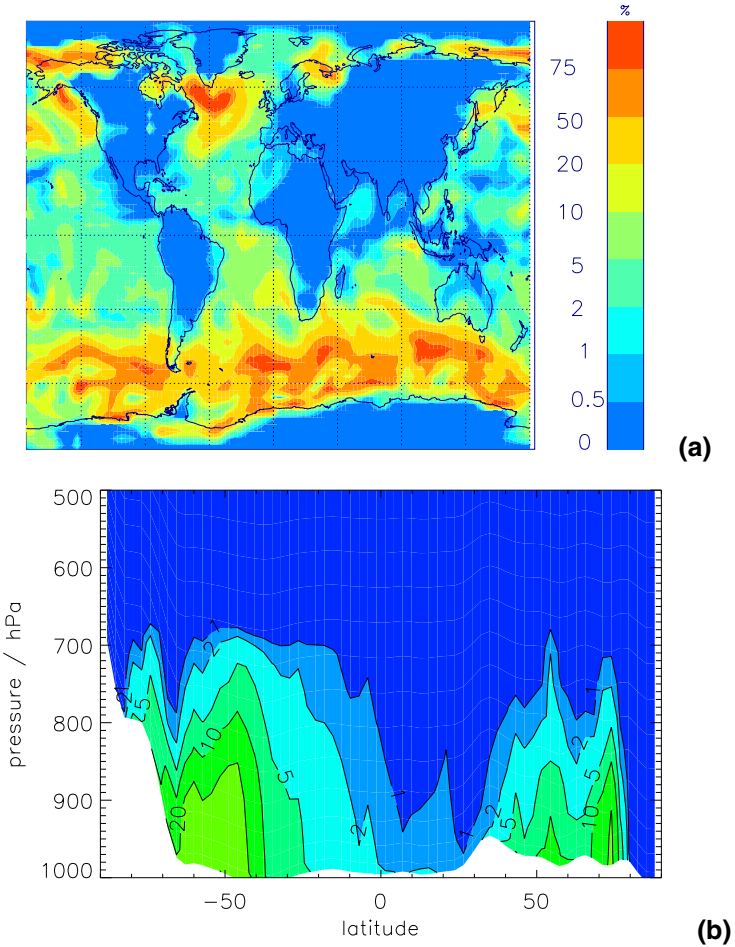

Fig. 9. Percentage contribution of sea spray to total CCN (at 0.2% supersaturation) for 1 December 1995 (24-h average) **(a)** Surface Level **(b)** Zonal mean.

ACPD
5, 179–215, 2005

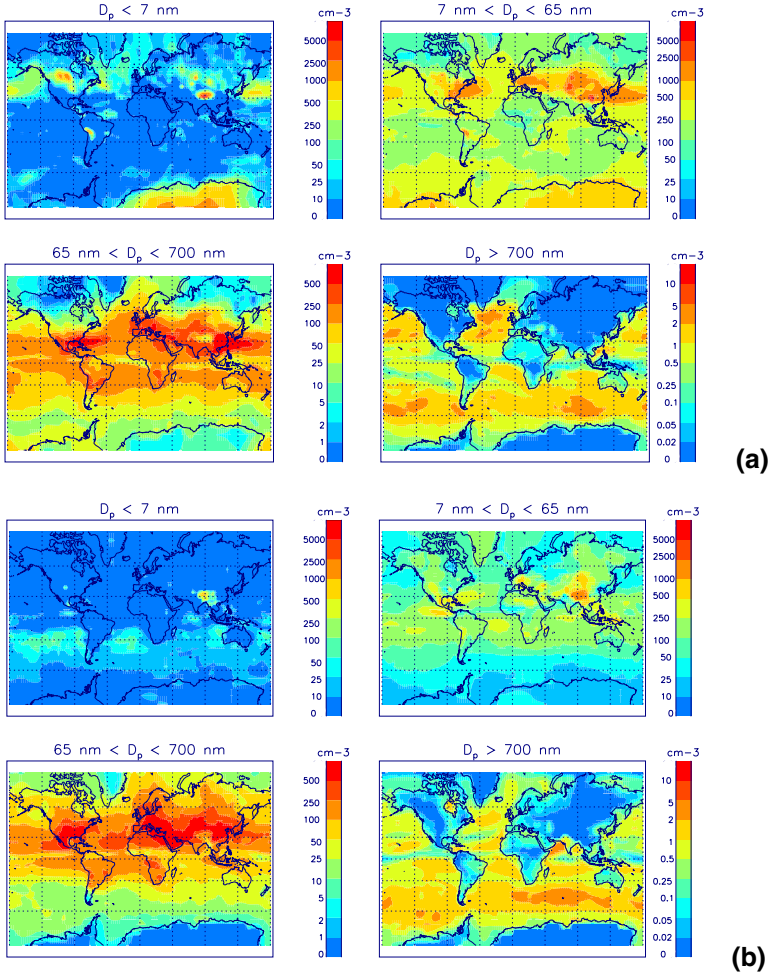

Fig. 10. Simulated monthly mean surface aerosol concentrations (cm^{-3}) for four dry aerosol diameter (D_p) size classes (at standard temperature and pressure) **(a)** December 1995 and **(b)** July 1997.

ACPD
5, 179–215, 2005

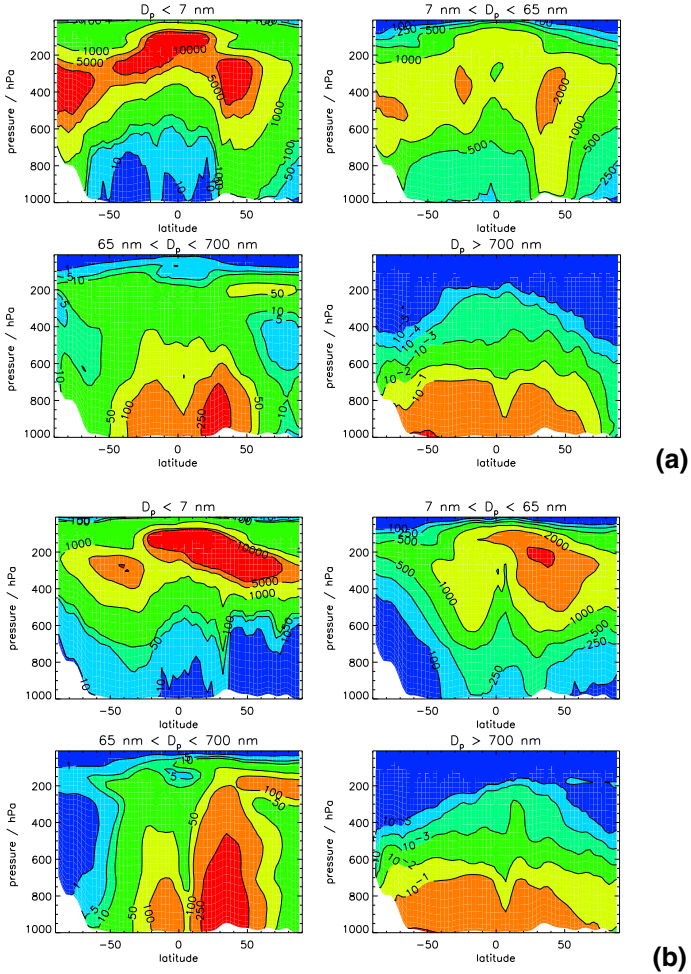

Fig. 11. Simulated monthly mean zonal aerosol concentrations (cm^{-3}) for four dry aerosol diameter (D_p) size classes (at standard temperature and pressure) **(a)** December 1995 and **(b)** July 1997.

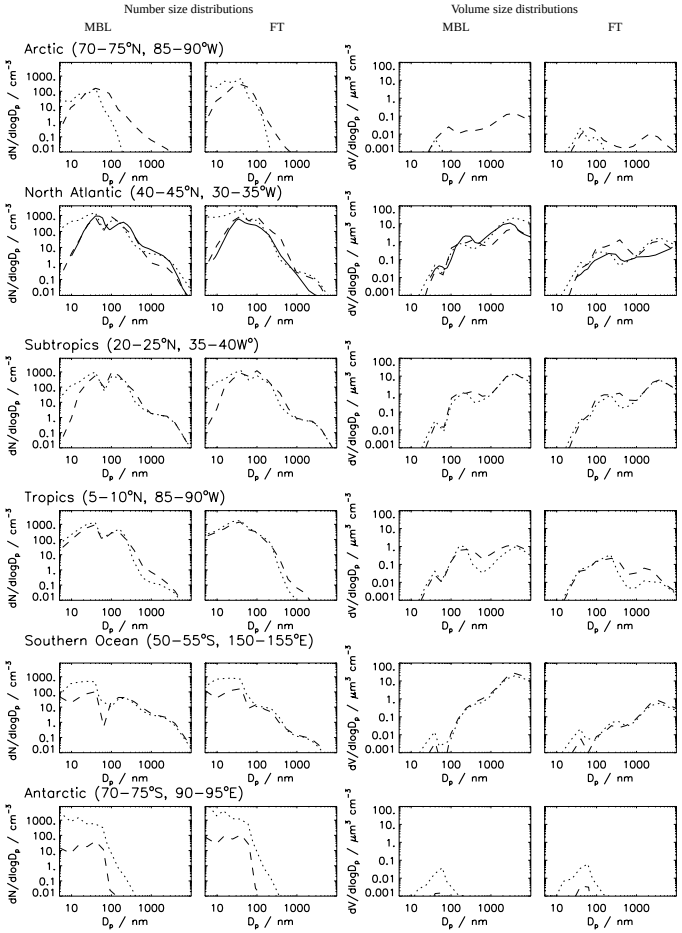

Fig. 12. Monthly averaged number and volume size distributions in the MBL and FT at various locations in December 1995 (dotted line) and July 1997 (dashed line). Observations (solid line) for the North Atlantic are from Raes et al. (2000).